Available online at www.sciencedirect.com
ScienceDirect
Journal of Computational Physics 219 (2006) 836–854
JOURNAL OF COMPUTATIONAL PHYSICS
www.elsevier.com/locate/jcp

Efficient and spectrally accurate numerical methods for computing ground and first excited states in Bose–Einstein condensates

Weizhu Bao [a,*], I-Liang Chern [b], Fong Yin Lim [a]

[a] *Department of Mathematics and Center of Computational Science and Engineering, National University of Singapore, 21 Lower Kent Ridge Road, Singapore 117543, Singapore*
[b] *Department of Mathematics, National Taiwan University, Taipei 106, Taiwan, ROC*

Received 20 December 2005; received in revised form 12 April 2006; accepted 28 April 2006
Available online 21 June 2006

Abstract

In this paper, we present two efficient and spectrally accurate numerical methods for computing the ground and first excited states in Bose–Einstein condensates (BECs). We begin with a review on the gradient flow with discrete normalization (GFDN) for computing stationary states of a nonconvex minimization problem and show how to choose initial data effectively for the GFDN. For discretizing the gradient flow, we use sine-pseudospectral method for spatial derivatives and either backward Euler scheme (BESP) or backward/forward Euler schemes for linear/nonlinear terms (BFSP) for temporal derivatives. Both BESP and BFSP are spectral order accurate for computing the ground and first excited states in BEC. Of course, they have their own advantages: (i) for linear case, BESP is energy diminishing for any time step size where BFSP is energy diminishing under a constraint on the time step size; (ii) at every time step, the linear system in BFSP can be solved directly via fast sine transform (FST) and thus it is extremely efficient, and in BESP it needs to be solved iteratively via FST by introducing a stabilization term and thus it could be efficient too. Comparisons between BESP and BFSP as well as other existing numerical methods are reported in terms of accuracy and total computational time. Our numerical results show that both BESP and BFSP are much more accurate and efficient than those existing numerical methods in the literature. Finally our new numerical methods are applied to compute the ground and first excited states in BEC in one dimension (1D), 2D and 3D with a combined harmonic and optical lattice potential for demonstrating their efficiency and high resolution.

Keywords: Bose–Einstein condensation; Gross–Pitaevskii equation; Energy; Ground state; First excited state; Normalized gradient flow

* Corresponding author.
E-mail addresses: bao@cz3.nus.edu.sg (W. Bao), chern@math.ntu.edu.tw (I-Liang Chern), fongyin.lim@nus.edu.sg (F.Y. Lim).
URLs: http://www.cz3.nus.edu.sg/~bao/ (W. Bao), http://www.math.ntu.edu.tw/~chern/ (I-Liang Chern).

0021-9991/$ - see front matter
doi:10.1016/j.jcp.2006.04.019

1. Introduction

The experimental realization of Bose–Einstein condensates (BECs) in magnetically trapped atomic gases at ultra-low temperature [3,15] has spurred great excitement in the atomic physics community and renewed the interest in studying the macroscopic quantum behavior of the atoms. Theoretical predictions of the properties of BEC like the density profile [10], collective excitations [18], and the formation of vortices [29] can now be compared with experimental data. This dramatic progress on the experimental front has stimulated a wave of activity on both the theoretical and the numerical front.

The properties of a BEC at temperature T much smaller than the critical condensation temperature T_c are well described by the macroscopic wave function $\psi(\mathbf{x},t)$, whose evolution is governed by a self-consistent, mean field nonlinear Schrödinger equation (NLSE), also known as the Gross–Pitaevskii equation (GPE) [22,27]:

$$\mathrm{i}\hbar\frac{\partial}{\partial t}\psi(\mathbf{x},t)=\left(-\frac{\hbar^2}{2m}\nabla^2+V(\mathbf{x})+NU_0|\psi(\mathbf{x},t)|^2\right)\psi(\mathbf{x},t),\quad \mathbf{x}\in\mathbb{R}^3,\ t>0, \tag{1.1}$$

where m is the atomic mass, $\hbar$ is the Planck constant, N is the number of atoms in the condensate, $V(\mathbf{x})$ is an external trapping potential, $U_0=\frac{4\pi\hbar^2 a_s}{m}$ describes the interaction between atoms in the condensate with a_s (positive for repulsive interaction and negative for attractive interaction) the s-wave scattering length. It is convenient to normalize the wave function by requiring

$$\|\psi(\cdot,t)\|^2:=\int_{\mathbb{R}^3}|\psi(\mathbf{x},t)|^2\,\mathrm{d}\mathbf{x}=1. \tag{1.2}$$

Under such a normalization and a given trapping potential, after proper nondimensionalization and dimension reduction in some limiting trapping frequency regimes, we can get the dimensionless GPE in the d-dimensions ($d=1,2,3$) [5,6,26,28]:

$$\mathrm{i}\frac{\partial}{\partial t}\psi(\mathbf{x},t)=\left(-\frac{1}{2}\nabla^2+V(\mathbf{x})+\beta|\psi(\mathbf{x},t)|^2\right)\psi(\mathbf{x},t),\quad \mathbf{x}\in\mathbb{R}^d,\ t>0, \tag{1.3}$$

where $V(\mathbf{x})$ is a real-valued potential whose shape is determined by the type of system under investigation, and positive/negative β corresponds to the repulsive/attractive interaction. In fact, in practical experiments, it is always in three dimensions (3D), i.e., $d=3$ in (1.3). For 1D and 2D GPE, the particles are tightly confined in the other dimensions. The condensate particles occupy only the ground state in the restricted directions. A 1D BEC can be realized in a cigar-shaped trap with two strongly confining axes and one weakly confining axis; a 2D BEC can be realized in a disk-shaped trap with one strongly confining axis and two weakly confining axes. For more details on nondimensionalization and dimension reduction for the GPE (1.1) as well as the physical meaning of 1D and 2D GPE, we refer to [7,6,8,28]. Two important invariants of (1.3) are the *normalization of the wave function*

$$N(\psi)=\|\psi(\cdot,t)\|^2=\int_{\mathbb{R}^d}|\psi(\mathbf{x},t)|^2\,\mathrm{d}\mathbf{x}=1,\quad t\geqslant 0 \tag{1.4}$$

and the *energy* per particle

$$E[\psi(\cdot,t)]=\int_{\mathbb{R}^d}\left[\frac{1}{2}|\nabla\psi(\mathbf{x},t)|^2+V(\mathbf{x})|\psi(\mathbf{x},t)|^2+\frac{\beta}{2}|\phi(\mathbf{x},t)|^4\right]\mathrm{d}\mathbf{x}. \tag{1.5}$$

To find a stationary solution of (1.3), we write

$$\psi(\mathbf{x},t)=\mathrm{e}^{-\mathrm{i}\mu t}\phi(\mathbf{x}), \tag{1.6}$$

where μ is the chemical potential of the condensate and ϕ is a real function independent of time. Inserting into (1.3) gives the equation

$$\mu\phi(\mathbf{x})=-\frac{1}{2}\nabla^2\phi(\mathbf{x})+V(\mathbf{x})\phi(\mathbf{x})+\beta|\phi(\mathbf{x})|^2\phi(\mathbf{x}),\quad \mathbf{x}\in\mathbb{R}^d, \tag{1.7}$$

for $\phi(\mathbf{x})$ under the normalization condition

$$\|\phi\|^2 := \int_{\mathbb{R}^d} |\phi(\mathbf{x})|^2 \, d\mathbf{x} = 1. \tag{1.8}$$

This is a nonlinear eigenvalue problem under a constraint, and any eigenvalue μ can be computed from its corresponding eigenfunction ϕ by

$$\mu = \mu(\phi) = \int_{\mathbb{R}^d} \left[\frac{1}{2} |\nabla \phi(\mathbf{x})|^2 + V(\mathbf{x}) |\phi(\mathbf{x})|^2 + \beta |\phi(\mathbf{x})|^4 \right] d\mathbf{x} = E(\phi) + \int_{\mathbb{R}^d} \frac{\beta}{2} |\phi(\mathbf{x})|^4 \, d\mathbf{x}.$$

In fact, the eigenfunctions of (1.7) under the constraint (1.8) are equivalent to the critical points of the energy functional $E(\phi)$ over the unit sphere $S = \{\phi \,|\, \|\phi\| = 1, \, E(\phi) < \infty\}$.

From mathematical point of view, the ground state of a BEC is defined as the minimizer of the following nonconvex minimization problem:

Find $(\mu_g, \phi_g \in S)$ such that

$$E_g := E(\phi_g) = \min_{\phi \in S} E(\phi), \quad \mu_g = \mu(\phi_g) = E_g + \int_{\mathbb{R}^d} \frac{\beta}{2} |\phi_g(\mathbf{x})|^4 \, d\mathbf{x}. \tag{1.9}$$

When $\beta \geqslant 0$ and $\lim_{|\mathbf{x}| \to \infty} V(\mathbf{x}) = \infty$, there exists a unique positive minimizer of the minimization problem (1.9) [26]. It is easy to show that the ground state ϕ_g is an eigenfunction of (1.7). Other eigenfunctions of (1.7) whose energies are larger than E_g are called as excited states in the physics literatures.

One of the fundamental problems in numerical simulation of BEC is to find its ground state so as to compare the numerical results with experimental observations and to prepare initial data for studying the dynamics of BEC. In fact, a BEC is formed when the particles occupy the lowest energy state, i.e., quantum mechanical ground state. In order to compute effectively the ground state of BEC, especially in the strong repulsive interaction regime and with optical lattice trapping potential [28,7], an efficient and accurate numerical method is one of the key issues. There has been a series of recent studies for developing numerical methods to compute the ground states in BEC. For example, Bao and Du [5] presented a continuous normalized gradient flow with diminishing energy and discretized it with a backward Euler finite difference (BEFD) and time-splitting sine-pseudospectral method (TSSP) for computing the ground and first excited states in BEC. This idea was extended to multi-component BEC [4] and rotating BEC [9]. Bao and Tang [8] proposed a method by directly minimizing the energy functional via finite element approximation to obtain the ground and excited states. Edwards and Burnett [17] presented a Runge–Kutta type method and used it to solve one and three-dimensional ground states with spherical symmetry. Adhikari [1] used this approach to get the ground state solution of GPE in 2D with radial symmetry. Ruprecht et al. [30] used the Crank–Nicolson finite difference method for solving BEC ground state. Chang et al. [11,12] proposed Gauss–Seidel-type methods for computing energy states of a multi-component BEC. Other approaches include an explicit imaginary-time algorithm used by Cerimele et al. [13] and Chiofalo et al. [14], a method based on time-independent GPE by Gammal et al. [19], a direct inversion in the iterated subspace (DIIS) used by Schneider et al. [31], and a simple analytical type method proposed by Dodd [16]. For convergence analysis of the finite dimensional approximation of (1.7), we refer to [33]. These numerical methods were applied to compute ground state in BEC with different trapping potentials [7,5,28].

For a BEC in an optical lattice or in a rotational frame, due to the oscillatory nature of the trapping potential or the appearance of quantized vortices, the ground and excited states are smooth but have multiscale structures [7]. Thus the resolution in space of a numerical method is essential for efficient computation, especially in 3D. In this case, all the numerical methods proposed in the literatures have some drawbacks: (i) The TSSP is explicit, conditionally stable and of spectral accuracy in space [5]. It is energy diminishing when time step satisfies a constraint. But due to the time-splitting error which does not vanishes at steady state, the time step must be chosen very small so as to get the ground state in high accuracy. Therefore, the total computational time is very large due to the small time step. (ii) The BEFD is implicit, unconditionally stable and energy diminishing for any time step, thus the time step can be chosen very large in practical computation. But it is only of second-order accuracy in space. When high accuracy is required or the solution has multiscale structures, much more grid points must be taken so as to get a

reasonable solution. Thus, the memory requirement is a big burden in this case. (iii) Other finite difference or finite element methods are usually of low order accuracy in space and in many cases they have a very severe constraint for time step due to stability or energy diminishing requirement [5]. Thus there are drawbacks in both TSSP and BEFD. The aim of this paper is to develop new numerical methods which enjoy the advantages of both TSSP and BEFD, i.e., they are spectrally accurate in space and are very efficient in terms of computational time. The key features of our numerical methods are based on: (i) the application of sine-pseudospectral discretization for spatial derivatives such that it is spectrally accurate; (ii) the adoption of backward Euler scheme (BESP) or backward/forward Euler scheme for linear/nonlinear terms for temporal derivatives such that they have good energy diminishing property; (iii) the introduction of a stabilization term with constant coefficient in BESP for accelerating convergence rate of the iterative method for a linear system or in BFSP for increasing upper bound of time step constraint; and (iv) the utilization of the fast sine transform (FST) as preconditioner for solving a linear system efficiently. Our extensive numerical results in 1D, 2D and 3D demonstrate that the methods are very accurate and efficient for computing the ground and first excited states in BEC.

The paper is organized as follows. In Section 2, we review the normalized gradient flow (NGF) for computing ground and first excited states, and discuss how to choose initial data for practical computation. In Section 3, we propose backward Euler sine-pseudospectral (BESP) method and backward/forward Euler sine-pseudospectral (BFSP) method for discretizing the NGF and discuss how to choose the 'optimal' stabilization parameter in the two schemes. Comparisons between BESP and BFSP as well as with existing numerical methods in the literature for computing ground states in BEC are reported in Section 4. Finally some conclusions are drawn in Section 5.

2. Normalized gradient flow and chosen initial data

For the convenience of readers, in this section, we will review the gradient flow with discrete normalization (GFDN) [5] for computing the minimizer of the minimization problem (1.9) and its energy diminishing property as well as how to choose initial data for computing the ground and first excited states in BEC [5].

2.1. Normalized gradient flow

Choose a time step $k = \Delta t > 0$ and set $t_n = n\Delta t$ for $n = 0,1,2,\ldots$ Applying the steepest decent method to the energy functional $E(\phi)$ without constraint (1.8), and then projecting the solution back to the unit sphere at the end of each time interval $[t_n, t_{n+1}]$ in order to satisfy the constraint (1.8), we obtain the following gradient flow with discrete normalization [2,5,13,14]:

$$\frac{\partial}{\partial t}\phi(\mathbf{x},t) = -\frac{1}{2}\frac{\delta E(\phi)}{\delta \phi} = \left(\frac{1}{2}\nabla^2 - V(\mathbf{x}) - \beta|\phi|^2\right)\phi(\mathbf{x},t), \quad \mathbf{x}\in\mathbb{R}^d,\ t_n \leqslant t < t_{n+1},\ n \geqslant 0, \tag{2.1}$$

$$\phi(\mathbf{x},t_{n+1}) := \phi(\mathbf{x},t_{n+1}^+) = \frac{\phi(\mathbf{x},t_{n+1}^-)}{\|\phi(\cdot,t_{n+1}^-)\|}, \quad \mathbf{x}\in\mathbb{R}^d,\ n \geqslant 0, \tag{2.2}$$

$$\phi(\mathbf{x},0) = \phi_0(\mathbf{x}), \quad \mathbf{x}\in\mathbb{R}^d \quad \text{with } \|\phi_0\| = 1, \tag{2.3}$$

where $\phi(\mathbf{x},t_n^{\pm}) = \lim_{t\to t_n^{\pm}}\phi(\mathbf{x},t)$. In fact, the gradient flow (2.1) can also be obtained from the GPE (1.3) by changing time t to imaginary time $\tau = \mathrm{i}t$. That's why the method is also called as imaginary time method in the physics literature [14,2].

When $\beta = 0$ and $V(\mathbf{x}) \geqslant 0$ for all $\mathbf{x}\in\mathbb{R}^d$, it was proved that the GFDN (2.1)–(2.3) is energy diminishing for any time step $\Delta t > 0$ and initial data ϕ_0 [5], i.e.,

$$E(\phi(\cdot,t_{n+1})) \leqslant E(\phi(\cdot,t_n)) \leqslant \cdots \leqslant E(\phi(\cdot,t_0)) = E(\phi_0), \quad n = 0,1,2,\ldots$$

which provides a rigorous mathematical justification for the algorithm to compute ground state in linear case. When $\beta > 0$, a similar argument is no longer valid [5]. However, letting $\Delta t \to 0$ in the GFDN (2.1)–(2.3), we obtain the following continuous normalized gradient flow (CNGF) [5]:

$$\partial_t \phi(\mathbf{x},t) = \left(\frac{1}{2}\nabla^2 - V(\mathbf{x}) - \beta|\phi|^2 + \frac{\mu(\phi(\cdot,t))}{\|\phi(\cdot,t)\|^2}\right)\phi(\mathbf{x},t), \quad \mathbf{x}\in\mathbb{R}^d,\ t\geqslant 0, \tag{2.4}$$

$$\phi(\mathbf{x},0) = \phi_0(\mathbf{x}), \quad \mathbf{x}\in\mathbb{R}^d \quad \text{with } \|\phi_0\| = 1. \tag{2.5}$$

This CNGF is normalization conserved and energy diminishing provided $\beta \geqslant 0$ and $V(\mathbf{x}) \geqslant 0$ for all $\mathbf{x}\in\mathbb{R}^d$ [5], i.e.,

$$\|\phi(\cdot,t)\|^2 \equiv \|\phi_0\|^2 = 1, \quad \frac{\mathrm{d}}{\mathrm{d}t}E(\phi(\cdot,t)) = -2\|\phi_t(\cdot,t)\|^2 \leqslant 0, \qquad t\geqslant 0,$$

which in turn implies that

$$E(\phi(\cdot,t_2)) \leqslant E(\phi(\cdot,t_1)), \quad 0\leqslant t_1\leqslant t_2 < \infty.$$

This provides a mathematical justification for the algorithm to compute ground state in nonlinear case at least when the time step Δt is small.

Due to the uniqueness of the positive ground state for non-rotating BEC [26], the ground state $\phi_g(\mathbf{x})$ and its corresponding chemical potential μ_g can be obtained from the steady state solution of the GFDN (2.1)–(2.3) or CNGF (2.4) and (2.5) provided that the initial data $\phi_0(\mathbf{x})$ is chosen as a positive function, i.e., $\phi_0(\mathbf{x}) \geqslant 0$ for $\mathbf{x}\in\mathbb{R}^d$. Furthermore, when $V(\mathbf{x})$ is an even function, the GFDN (2.1)–(2.3) can also be applied to compute the first excited state in BEC provided that the initial data $\phi_0(\mathbf{x})$ is chosen to be an odd function [5]. In order to compute the ground and first excited states in BEC efficiently and accurately, we will discuss how to choose proper initial data $\phi_0(\mathbf{x})$ for different parameter regimes in the following subsection and propose BESP and BFSP for discretizing the GFDN (2.1)–(2.3) in the following section.

2.2. Chosen initial data for the normalized gradient flow

In order to save computational cost, proper initial data for the GFDN (2.1)–(2.3) is one of the key issues for computing the ground state. Without lose of generality, we assume the trapping potential $V(\mathbf{x})$ in (1.3) satisfying

$$V(\mathbf{x}) = V_0(\mathbf{x}) + W(\mathbf{x}), \qquad V_0(\mathbf{x}) = \frac{1}{2}(\gamma_1^2 x_1^2 + \cdots + \gamma_d^2 x_d^2), \quad \lim_{|\mathbf{x}|\to+\infty}\frac{W(\mathbf{x})}{V_0(\mathbf{x})} = 0, \tag{2.6}$$

where $\mathbf{x} = (x_1,\ldots,x_d)^{\mathrm{T}} \in \mathbb{R}^d$ and $\gamma_j > 0$ for $1\leqslant j\leqslant d$. Typical example for $W(\mathbf{x})$ is the optical lattice potential [7,28]

$$W(\mathbf{x}) = k_1\sin^2(q_1x_1^2) + \cdots + k_d\sin^2(q_dx_d^2)$$

with k_j and q_j $(1\leqslant j\leqslant d)$ positive constants. In this case, when $|\beta|$ is not big, e.g. $|\beta| < 10$, a possible choice of the initial data is to choose the ground state of (1.3) with $\beta = 0$ and $V(\mathbf{x}) = V_0(\mathbf{x})$ [28,6,8], i.e.,

$$\phi_0(\mathbf{x}) = \frac{\left(\prod_{j=1}^d \gamma_j\right)^{1/4}}{\pi^{d/4}}\exp[-(\gamma_1x_1^2 + \cdots + \gamma_dx_d^2)], \quad \mathbf{x}\in\mathbb{R}^d. \tag{2.7}$$

On the other hand, when $|\beta|$ is not small, e.g. $|\beta| \geqslant 10$, a possible choice of the initial data is to choose the Thomas–Fermi approximation [6,7]:

$$\phi_0(\mathbf{x}) = \frac{\phi_g^{\mathrm{TF}}(\mathbf{x})}{\|\phi_g^{\mathrm{TF}}\|}, \quad \phi_g^{\mathrm{TF}}(\mathbf{x}) = \begin{cases}\sqrt{\frac{\mu_g^{\mathrm{TF}} - V(\mathbf{x})}{\beta}}, & V_0(\mathbf{x}) < \mu_g^{\mathrm{TF}},\\ 0, & \text{otherwise},\end{cases} \quad \mathbf{x}\in\mathbb{R}^d, \tag{2.8}$$

where

$$\mu_g^{\mathrm{TF}} = \frac{1}{2}\begin{cases}(3\beta\gamma_1)^{2/3}, & d=1,\\ (4\beta\gamma_1\gamma_2)^{1/2}, & d=2,\\ (15\beta\gamma_1\gamma_2\gamma_3/4\pi)^{2/5}, & d=3.\end{cases}$$

3. Efficient and accurate numerical methods

In this section, we will propose BESP and BFSP for fully discretizing the GFDN (2.1)–(2.3) and discuss how to choose the 'optimal' stabilization parameter in the two schemes.

Due to the trapping potential $V(\mathbf{x})$ given by (2.6), the solution $\phi(\mathbf{x},t)$ of (2.1)–(2.3) decays to zero exponentially fast when $|\mathbf{x}| \to \infty$. Thus in practical computation, we truncate the problem (2.1)–(2.3) into a bounded computational domain with homogeneous Dirichlet boundary conditions:

$$\frac{\partial}{\partial t}\phi(\mathbf{x},t) = \left(\frac{1}{2}\nabla^2 - V(\mathbf{x}) - \beta|\phi|^2\right)\phi(\mathbf{x},t), \quad \mathbf{x} \in \Omega_{\mathbf{x}},\ t_n \leqslant t < t_{n+1},\ n \geqslant 0, \tag{3.1}$$

$$\phi(\mathbf{x},t_{n+1}) = \frac{\phi(\mathbf{x},t_{n+1}^-)}{\|\phi(\cdot,t_{n+1}^-)\|}, \quad \mathbf{x} \in \Omega_{\mathbf{x}},\ n \geqslant 0, \tag{3.2}$$

$$\phi(\mathbf{x},t) = 0, \quad \mathbf{x} \in \Gamma = \partial\Omega_{\mathbf{x}},\ t > 0, \tag{3.3}$$

$$\phi(\mathbf{x},0) = \phi_0(\mathbf{x}), \quad \mathbf{x} \in \Omega_{\mathbf{x}} \quad \text{with } \|\phi_0\|^2 := \int_{\Omega_{\mathbf{x}}} |\phi_0(\mathbf{x})|^2 \,\mathrm{d}\mathbf{x} = 1, \tag{3.4}$$

where we choose $\Omega_{\mathbf{x}}$ as an interval (a,b) in 1D, a rectangle $(a,b)\times(c,d)$ in 2D, and a box $(a,b)\times(c,d)\times(e,f)$ in 3D, with $|a|$, $|c|$, $|e|$, b, d and f sufficiently large.

For simplicity of notation we shall introduce the method in 1D, i.e., $d = 1$ in (3.1)–(3.4). Generalization to $d > 1$ is straightforward for tensor product grids and the results remain valid without modifications. For 1D, we choose the spatial mesh size $h = \Delta x > 0$ with $h = (b-a)/M$ for M an even positive integer, and let the grid points be

$$x_j := a + jh, \quad j = 0, 1, \ldots, M.$$

Let ϕ_j^n be the approximation of $\phi(x_j,t_n)$ and ϕ^n be the solution vector with component ϕ_j^n.

3.1. Backward Euler sine-pseudospectral method

In order to discretize the gradient flow (3.1) with $d = 1$, we use backward Euler method for time discretization and sine-pseudospectral method for spatial derivatives (BESP). The detailed scheme is:

$$\frac{\phi_j^* - \phi_j^n}{\Delta t} = \frac{1}{2} D_{xx}^s \phi^*|_{x=x_j} - V(x_j)\phi_j^* - \beta|\phi_j^n|^2\phi_j^*, \quad j = 1, 2, \ldots, M-1, \tag{3.5}$$

$$\phi_0^* = \phi_M^* = 0, \quad \phi_j^0 = \phi_0(x_j),\ j = 0, 1, \ldots, M, \tag{3.6}$$

$$\phi_j^{n+1} = \frac{\phi_j^*}{\|\phi^*\|}, \quad j = 0, 1, \ldots, M,\ n = 0, 1, \ldots \tag{3.7}$$

where the norm is designed as $\|\phi^*\|^2 = h\sum_{j=1}^{M-1}|\phi_j^*|^2$. Here D_{xx}^s, a spectral differential operator approximation of ∂_{xx}, is defined as

$$D_{xx}^s U|_{x=x_j} = -\frac{2}{M}\sum_{l=1}^{M-1} \mu_l^2 (\hat{U})_l \sin(\mu_l(x_j - a)), \quad j = 1, 2, \ldots, M-1,$$

where $(\hat{U})_l$ $(l = 1, 2, \ldots, M-1)$, the sine transform coefficients of the vector $U = (U_0, U_1, \ldots, U_M)^{\mathrm{T}}$ satisfying $U_0 = U_M = 0$, are defined as

$$\mu_l = \frac{\pi l}{b-a}, \qquad (\hat{U})_l = \sum_{j=1}^{M-1} U_j \sin(\mu_l(x_j - a)), \quad l = 1, 2, \ldots, M-1.$$

In the discretization (3.5), at every time step, a linear system has to be solved. Here we present an efficient way to solve it iteratively by introducing a stabilization term with constant coefficient and using discrete sine transform:

$$\frac{\phi_j^{*,m+1}-\phi_j^n}{\Delta t}=\frac{1}{2}D_{xx}^{s}\phi^{*,m+1}|_{x=x_j}-\alpha\phi_j^{*,m+1}+(\alpha-V(x_j)-\beta|\phi_j^n|^2)\phi_j^{*,m},\quad m\geqslant 0, \tag{3.8}$$

$$\phi_j^{*,0}=\phi_j^n,\quad j=0,1,\ldots,M, \tag{3.9}$$

where $\alpha\geqslant 0$ is called as a stabilization parameter to be determined. Taking discrete sine transform at both sides of (3.8), we obtain

$$\frac{(\widehat{\phi^{*,m+1}})_l-(\widehat{\phi^n})_l}{\Delta t}=-\left(\alpha+\frac{1}{2}\mu_l^2\right)(\widehat{\phi^{*,m+1}})_l+(\widehat{G^m})_l,\quad l=1,2,\ldots,M-1, \tag{3.10}$$

where $(\widehat{G^m})_l$ are the sine transform coefficients of the vector $G^m=(G_0^m,G_1^m,\ldots,G_M^m)^{\mathrm{T}}$ defined as

$$G_j^m=(\alpha-V(x_j)-\beta|\phi_j^n|^2)\phi_j^{*,m},\quad j=0,1,\ldots,M. \tag{3.11}$$

Solving (3.10), we get

$$(\widehat{\phi^{*,m+1}})_l=\frac{2}{2+\Delta t(2\alpha+\mu_l^2)}[(\widehat{\phi^n})_l+\Delta t(\widehat{G^m})_l],\quad l=1,2,\ldots,M-1. \tag{3.12}$$

Taking inverse discrete sine transform for (3.12), we get the solution for (3.8) immediately.

In order to find the 'optimal' stabilization parameter α in (3.8) such that the iterative method (3.8) for solving (3.5) converges as fast as possible, we write it into a matrix form

$$A\phi^{*,m+1}=B\phi^{*,m}+C,\quad m=0,1,\ldots, \tag{3.13}$$

where

$$A=(1+\alpha\Delta t)I-\frac{\Delta t}{2}D_{xx}^{s},\quad C=\mathrm{diag}(\phi_1^n,\ldots,\phi_{M-1}^n), \tag{3.14}$$

$$B=\Delta t\,\mathrm{diag}(\alpha-V(x_1)-\beta|\phi_1^n|^2,\ldots,\alpha-V(x_{M-1})-\beta|\phi_{M-1}^n|^2) \tag{3.15}$$

with I an $(M-1)\times(M-1)$ identity matrix. Since A is a positive definite matrix, by the standard theory for iterative method for a linear system [20], a sufficient and necessary condition for the convergence of the iterative method is

$$\rho(A^{-1}B)<1, \tag{3.16}$$

where $\rho(D)$ is the spectral radius of the matrix D. Plugging (3.14) and (3.15) into (3.16), we obtain

$$\begin{aligned}\rho(A^{-1}B)&\leqslant\|A^{-1}B\|_2\leqslant\|A^{-1}\|_2\|B\|_2=\frac{\Delta t\max_{1\leqslant j\leqslant M-1}|\alpha-V(x_j)-\beta|\phi_j^n|^2|}{1+\alpha\Delta t+\frac{\Delta t}{2}\min_{1\leqslant l\leqslant M-1}\mu_l^2}\\&=\frac{\Delta t\max\{|\alpha-b_{\max}|,|\alpha-b_{\min}|\}}{1+\alpha\Delta t+\frac{\pi^2\Delta t}{2(b-a)^2}},\end{aligned} \tag{3.17}$$

where

$$b_{\max}=\max_{1\leqslant j\leqslant M-1}(V(x_j)+\beta|\phi_j^n|^2),\quad b_{\min}=\min_{1\leqslant j\leqslant M-1}(V(x_j)+\beta|\phi_j^n|^2). \tag{3.18}$$

Therefore, if we take the stabilization parameter α as

$$\alpha_{\mathrm{opt}}=\frac{1}{2}(b_{\max}+b_{\min}), \tag{3.19}$$

we get

$$\rho(A^{-1}B)\leqslant\frac{\Delta t\max\{|\alpha_{\mathrm{opt}}-b_{\max}|,|\alpha_{\mathrm{opt}}-b_{\min}|\}}{1+\alpha_{\mathrm{opt}}\Delta t+\frac{\pi^2\Delta t}{2(b-a)^2}}\leqslant\frac{\Delta t(b_{\min}+b_{\max})}{2+\Delta t(b_{\min}+b_{\max})+\frac{\pi^2\Delta t}{(b-a)^2}}<1,$$

which guarantees the convergence of the iterative method (3.8) and the convergent rate is 'optimal' as

$$R(A^{-1}B) := -\ln \rho(A^{-1}B) \geqslant \ln \frac{2 + \Delta t(b_{\min} + b_{\max}) + \frac{\pi^2 \Delta t}{(b-a)^2}}{\Delta t(b_{\min} + b_{\max})}. \tag{3.20}$$

For the convenience of the reader, an algorithm for implementing BESP is attached in Appendix A.

3.2. Backward/forward Euler sine-pseudospectral method

Since ϕ^{n+1} in (3.7), i.e., ϕ^* in (3.5), is just an intermediate approximation for the ground state solution, there is no need to solve the linear system (3.5) for ϕ^* very accurately. Specifically, if we only iterate (3.8) for one step, the algorithm is significantly simplified. In fact, this is equivalent to use sine-pseudospectral method for spatial derivatives and backward/forward Euler scheme for linear/nonlinear terms in time derivatives (BFSP) for discretizing the gradient flow (3.1) with $d = 1$. The detailed scheme is:

$$\frac{\phi_j^* - \phi_j^n}{\Delta t} = \frac{1}{2} D_{xx}^s \phi^*|_{x=x_j} - \alpha \phi_j^* + (\alpha - V(x_j) - \beta|\phi_j^n|^2)\phi_j^n, \quad 1 \leqslant j < M, \tag{3.21}$$

$$\phi_0^* = \phi_M^* = 0, \quad \phi_j^0 = \phi_0(x_j), \qquad j = 0, 1, \ldots, M, \tag{3.22}$$

$$\phi_j^{n+1} = \frac{\phi_j^*}{\|\phi^*\|}, \qquad j = 0, 1, \ldots, M, \quad n = 0, 1, \ldots \tag{3.23}$$

where $\alpha \geqslant 0$ is the stabilization parameter. This discretization is implicit, but it can be solved directly via fast discrete sine transform. Thus it is extremely efficient in practical computation. In fact, the memory requirement is $O(M)$ and computational cost per time step is $O(M\ln(M))$. Of course, there is a constraint for time step such that the flow is energy diminishing. By Remark 2.13 in [5], the constraint for time step Δt is

$$\Delta t < \frac{1}{\max_{1 \leqslant j \leqslant M-1} |\alpha - V(x_j) - \beta|\phi_j^n|^2|} = \frac{1}{\max\{|\alpha - b_{\min}|, |\alpha - b_{\max}|\}}.$$

Therefore, if we take $\alpha = \alpha_{\text{opt}} = \frac{b_{\max} + b_{\min}}{2}$, the bound in the constraint for Δt is 'optimal'. In this case, it reads

$$\Delta t < \frac{2}{b_{\min} + b_{\max}}.$$

Again, for the convenience of the reader, an algorithm for implementing BFSP is attached in Appendix B.

3.3. Other discretization schemes

For comparison purposes we review alternative discretization schemes for discretizing the gradient flow (3.1)–(3.4). One is the forward Euler sine-pseudospectral (FESP) scheme:

$$\frac{\phi_j^* - \phi_j^n}{\Delta t} = \frac{1}{2} D_{xx}^s \phi^n|_{x=x_j} - V(x_j)\phi_j^n - \beta|\phi_j^n|^2 \phi_j^n, \quad j = 1, 2, \ldots, M-1. \tag{3.24}$$

By Remark 2.13 in [5], the constraint for time step Δt is

$$\Delta t < \frac{2}{2b_{\max} + \mu_{M-1}^2} = \frac{2}{2b_{\max} + (M-1)^2\pi^2/(b-a)^2} < \frac{2h^2}{\pi^2 + 2h^2 b_{\max}}.$$

Another one is the backward Euler finite difference (BEFD) scheme, which is unconditionally stable and proposed in [5]

$$\frac{\phi_j^* - \phi_j^n}{\Delta t} = \frac{\phi_{j-1}^* - 2\phi_j^* + \phi_{j+1}^*}{2h^2} - V(x_j)\phi_j^* - \beta|\phi_j^n|^2\phi_j^*, \quad j = 1, 2, \ldots, M-1. \tag{3.25}$$

This discretization is only second order as demonstrated in [5].

4. Numerical results

In this section, we demonstrate the spectral accuracy in space for our new methods BESP (3.5)–(3.7) and BFSP (3.21)–(3.23) for computing the ground and first excited states in BEC, and perform numerical comparisons between BESP and BFSP as well as existing numerical methods, e.g. BEFD, in terms of spatial accuracy and computational time. Then we apply the methods BESP and BFSP to compute the ground and first excited states in BEC in 1D, 2D and 3D for different trapping potential, especially in optical lattice potential. The parameters chosen in our numerical examples are motivated from the physics literatures [21,24,25,23] such that the GPE is valid for either describing the atomic gas or dynamics of nonlinear optics. The main aim of the numerical study in this paper is to test and demonstrate the spectral accuracy in space of our new numerical methods. For the validity of the GPE when a transition from a BEC state to a Mott insulator state taking place at a certain depth of the lattice, we refer to [21,24].

4.1. Comparisons of spatial accuracy and results in 1D

Example 1. Ground and first excited states in 1D, i.e., we take $d = 1$ in (1.3) and study two kinds of trapping potentials:

Case I.
A harmonic oscillator potential $V(x) = \frac{x^2}{2}$ and $\beta = 400$ in (1.3).

Case II.
An optical lattice potential $V(x) = \frac{x^2}{2} + 25\sin^2\left(\frac{\pi x}{4}\right)$ and $\beta = 250$ in (1.3).

The values of the optical lattice and nonlinearity are motivated from the physics literatures [21,25,32,23]. The initial data (3.4) is chosen as (2.8) for computing the ground state, and, respectively, $\phi_0(x) = \frac{\sqrt{2}x}{\pi^{1/4}}e^{-x^2/2}$ for computing the first excited state. We solve the problem with BESP on $[-16, 16]$, i.e., $a = -16$ and $b = 16$, and take time step $\Delta t = 0.05$ for computing the ground state, and, respectively, $\Delta t = 0.001$ for computing the first excited state. Here and in the next two examples, the reason for smaller time step chosen for computing the first excited states is to suppress the round-off error in fast sine transform (FST) and inverse fast sine transform (IFST) such that the numerical solution is an odd function. In our computations in this section, the termination condition for solving the linear system (3.5) by (3.8) is $\max_{1\leqslant j\leqslant M-1} |\phi_j^{*,m+1} - \phi_j^{*,m}| < 10^{-13}$, and the steady state solution of BESP is reached when $\max_{1\leqslant j\leqslant M-1} |\phi_j^{n+1} - \phi_j^n| < 10^{-12}$. Let ϕ_g and ϕ_1 be the 'exact' ground state and first excited state which are obtained numerically by using BESP with a very fine mesh $h = \frac{1}{32}$ and $h = \frac{1}{128}$, respectively. We denote their energy and chemical potential as $E_g := E(\phi_g)$, $E_1 := E(\phi_1)$, and $\mu_g := \mu(\phi_g)$, $\mu_1 := \mu(\phi_1)$. Let $\phi_{g,h}^{SP}$ and $\phi_{1,h}^{SP}$ be the numerical ground state and first excited state obtained by using BESP with mesh size h, respectively. Similarly, $\phi_{g,h}^{FD}$ and $\phi_{1,h}^{FD}$ are obtained by using BEFD in a similar way. Tables 1 and 2 list the errors for Case I, and Tables 3 and 4 for Case II. Furthermore, we also compute the energy and chemical potential for the ground state and first excited states based on our 'exact' solution ϕ_g and ϕ_1. For Case I, we have $E_g := E(\phi_g) = 21.3601$ and $\mu_g := \mu(\phi_g) = 35.5775$ for ground state, and $E_1 := E(\phi_1) = 22.0777$ and $\mu_1 := \mu(\phi_1) = 36.2881$ for the first excited state. Similarly, for Case II, we have $E_g = 26.0838$, $\mu_g = 38.0692$, $E_1 = 27.3408$ and $\mu_1 = 38.9195$. Fig. 1 plots ϕ_g and ϕ_1 as well as their corresponding trapping potentials for Cases I and II.

From Tables 1–4, Fig. 1 and additional experiments not shown here, the following observations are made:

(i) For BESP, BFSP and FESP, they are spectrally accurate in spatial discretization; where for BEFD, it is only second-order accurate. The error in the ground and first excited states is only due to the spatial discretization. In fact, we also find how fine the mesh size h should be for the BEFD so as to achieve very high accuracy. For Case I, we have $\max|\phi_g - \phi_{g,h}^{FD}| = 1.4 \times 10^{-11}$ and $|E_g - E(\phi_{g,h}^{FD})| = 8 \times 10^{-12}$ for mesh size $h = 1/32768$; and $\max|\phi_1 - \phi_{1,h}^{FD}| = 2.68 \times 10^{-10}$ and $|E_1 - E(\phi_{1,h}^{FD})| = 8.30 \times 10^{-10}$ for mesh

Table 1
Spatial resolution of BESP and BEFD for ground state of Case I in Example 1

Mesh size	$h = 1$	$h = 1/2$	$h = 1/4$	$h = 1/8$
$\max\|\phi_g - \phi_{g,h}^{SP}\|$	1.310E − 3	7.037E − 5	1.954E − 8	<E − 12
$\|\phi_g - \phi_{g,h}^{SP}\|$	1.975E − 3	7.425E − 5	2.325E − 8	<E − 12
$\|E_g - E(\phi_{g,h}^{SP})\|$	5.688E − 5	2.642E − 6	9E − 12	<E − 12
$\|\mu_g - \mu(\phi_{g,h}^{SP})\|$	1.661E − 2	8.705E − 5	9.44E − 10	4E − 12
$\max\|\phi_g - \phi_{g,h}^{FD}\|$	2.063E − 3	1.241E − 3	2.890E − 4	7.542E − 5
$\|\phi_g - \phi_{g,h}^{FD}\|$	3.825E − 3	1.439E − 3	3.130E − 4	7.705E − 5
$\|E_g - E(\phi_{g,h}^{FD})\|$	2.726E − 3	9.650E − 4	2.540E − 4	6.439E − 5
$\|\mu_g - \mu(\phi_{g,h}^{FD})\|$	2.395E − 2	6.040E − 4	2.240E − 4	5.694E − 5

Table 2
Spatial resolution of BESP and BEFD for the first excited state of Case I in Example 1

Mesh size	$h = 1/4$	$h = 1/8$	$h = 1/16$	$h = 1/32$
$\max\|\phi_1 - \phi_{1,h}^{SP}\|$	2.064E − 1	6.190E − 4	2.099E − 7	<E − 12
$\|\phi_1 - \phi_{1,h}^{SP}\|$	1.093E − 1	3.200E − 4	1.403E − 7	<E − 12
$\|E_1 - E(\phi_{1,h}^{SP})\|$	5.259E − 2	3.510E − 4	5.550E − 9	<E − 12
$\|\mu_1 - \mu(\phi_{1,h}^{SP})\|$	1.216E − 1	1.509E − 3	4.762E − 8	<E − 12
$\max\|\phi_1 - \phi_{1,h}^{FD}\|$	2.348E − 1	8.432E − 3	2.267E − 3	6.040E − 4
$\|\phi_1 - \phi_{1,h}^{FD}\|$	1.197E − 1	4.298E − 3	1.215E − 3	2.950E − 4
$\|E_1 - E(\phi_{1,h}^{FD})\|$	3.154E − 1	5.212E − 2	1.382E − 2	3.449E − 3
$\|\mu_1 - \mu(\phi_{1,h}^{FD})\|$	4.216E − 1	5.884E − 2	1.609E − 2	3.999E − 3

Table 3
Spatial resolution of BESP and BEFD for ground state of Case II in Example 1

Mesh size	$h = 1$	$h = 1/2$	$h = 1/4$	$h = 1/8$
$\max\|\phi_g - \phi_{g,h}^{SP}\|$	7.982E − 3	1.212E − 3	2.219E − 6	1.9E − 11
$\|\phi_g - \phi_{g,h}^{SP}\|$	1.304E − 2	1.313E − 3	2.431E − 6	2.8E − 11
$\|E_g - E(\phi_{g,h}^{SP})\|$	4.222E − 4	1.957E − 4	4.994E − 8	<E − 12
$\|\mu_g - \mu(\phi_{g,h}^{SP})\|$	9.761E − 2	4.114E − 3	5.605E − 7	<E − 12
$\max\|\phi_g - \phi_{g,h}^{FD}\|$	1.019E − 2	5.815E − 3	1.001E − 3	2.541E − 4
$\|\phi_g - \phi_{g,h}^{FD}\|$	1.967E − 2	7.051E − 3	1.390E − 3	3.387E − 4
$\|E_g - E(\phi_{g,h}^{FD})\|$	7.852E − 2	2.961E − 2	7.940E − 3	2.027E − 3
$\|\mu_g - \mu(\phi_{g,h}^{FD})\|$	1.786E − 1	1.716E − 2	6.730E − 3	1.728E − 3

Table 4
Spatial resolution of BESP and BEFD for the first excited state of Case II in Example 1

Mesh size	$h = 1/4$	$h = 1/8$	$h = 1/16$	$h = 1/32$
$\max\|\phi_1 - \phi_{1,h}^{SP}\|$	2.793E − 1	1.010E − 3	4.240E − 7	2E − 12
$\|\phi_1 - \phi_{1,h}^{SP}\|$	1.477E − 1	5.241E − 4	2.784E − 7	2E − 12
$\|E_1 - E(\phi_{1,h}^{SP})\|$	1.145E − 1	8.337E − 4	1.943E − 8	<E − 12
$\|\mu_1 - \mu(\phi_{1,h}^{SP})\|$	1.593E − 1	2.357E − 3	1.097E − 7	5E − 12
$\max\|\phi_1 - \phi_{1,h}^{FD}\|$	3.134E − 1	1.124E − 2	3.231E − 3	8.450E − 4
$\|\phi_1 - \phi_{1,h}^{FD}\|$	1.599E − 1	5.779E − 3	1.701E − 3	4.122E − 4
$\|E_1 - E(\phi_{1,h}^{FD})\|$	6.011E − 1	1.002E − 1	2.688E − 2	6.707E − 3
$\|\mu_1 - \mu(\phi_{1,h}^{FD})\|$	6.315E − 1	9.887E − 2	2.742E − 2	6.827E − 3

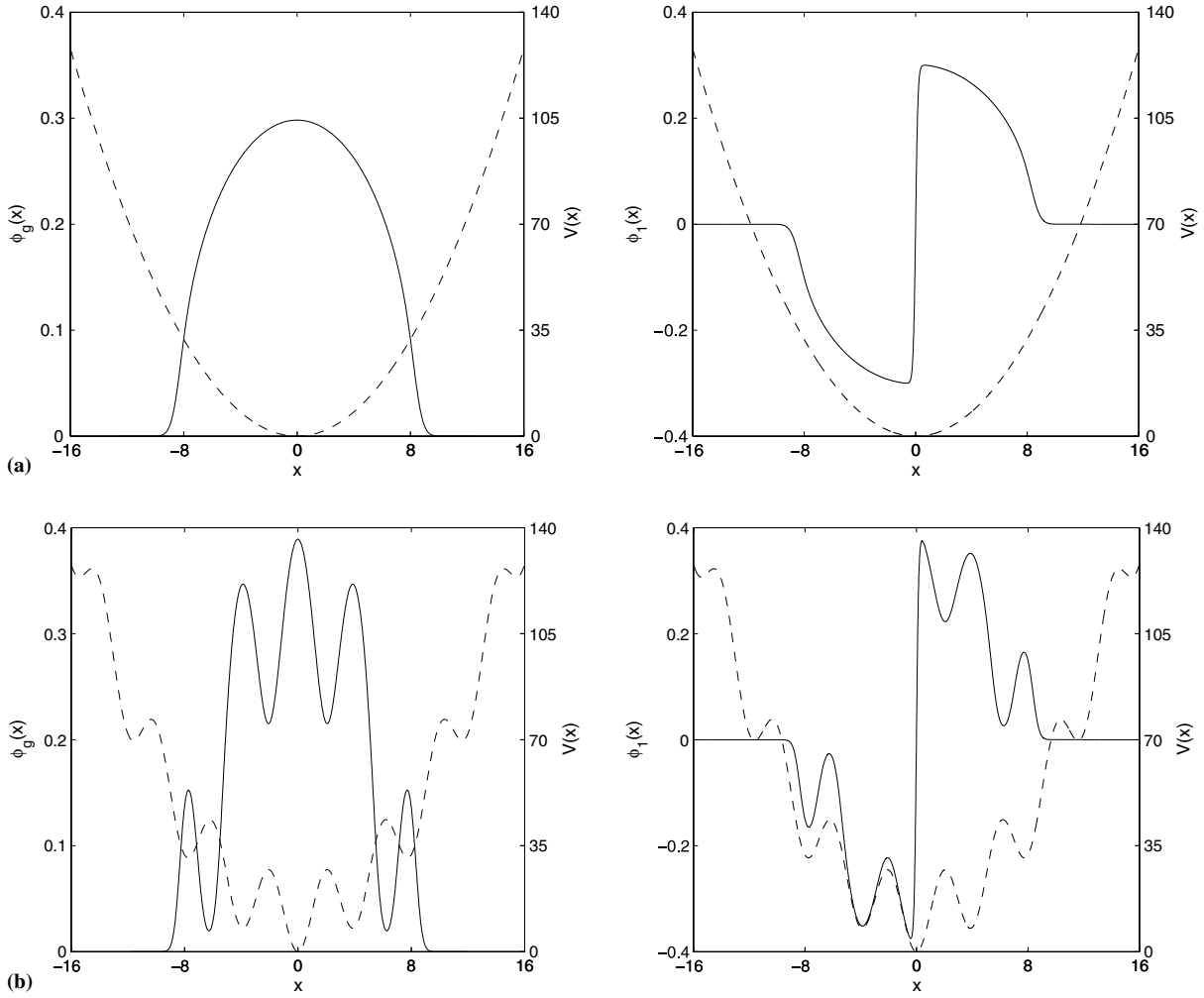

Fig. 1. Ground state ϕ_g (left column, solid lines) and first excited state ϕ_1 (right column, solid lines) as well as trapping potentials (dashed lines) in Example 1: (a) for Case I; (b) for Case II.

size $h = 1/65536$. Similarly, for Case II, we have $\max|\phi_g - \phi_{g,h}^{FD}| = 2.3 \times 10^{-11}$ and $|E_g - E(\phi_{g,h}^{FD})| = 1.23 \times 10^{-10}$ for mesh size $h = 1/32768$. Thus when high accuracy is required or the solution has multi-scale structure [7], BESP and BFSP are much better than BEFD in terms that they need much less grid points. Therefore BESP and BFSP can save a lot of memory and computational time, especially in 2D and 3D.

(ii) Interior layers are observed in the first excited state when β is large (cf. Fig. 1 'right column'). When an optical lattice potential is applied, multiscale structures are observed in both ground and first excited states (cf. Fig. 1b).

(iii) In both the two different potentials, we observed numerically

$$E(\phi_g) < E(\phi_1), \quad \mu(\phi_g) < \mu(\phi_1) \quad \text{for any } \beta \geqslant 0,$$

$$\lim_{\beta\to\infty} \frac{E(\phi_1)}{E(\phi_g)} = 1, \quad \lim_{\beta\to\infty} \frac{\mu(\phi_1)}{\mu(\phi_g)} = 1.$$

These results agree with the observation in [5,7,8] very well.

4.2. Comparisons of computational time and results in 2D

Example 2. Ground and first excited states in 2D under a combined harmonic and optical lattice potential, i.e., we take $d = 2$ and $V(x,y) = \frac{1}{2}(x^2+y^2) + \kappa\left[\sin^2(\frac{\pi x}{4}) + \sin^2(\frac{\pi y}{4})\right]$ in (1.3). The choice of the optical lattice depth and nonlinearity is motivated from the physics literatures [21,25,23]. The initial data (3.4) is chosen as (2.8) for computing ground state ϕ_g, and as $\phi_0(x,y) = \frac{\sqrt{2}x}{\pi^{1/2}} e^{-(x^2+y^2)/2}$ for the first excited state in x-direction ϕ_{10}, and as $\phi_0(x,y) = \frac{\sqrt{2}y}{\pi^{1/2}} e^{-(x^2+y^2)/2}$ for the first excited state in y-direction ϕ_{01}, and as $\phi_0(x,y) = \frac{2xy}{\pi^{1/2}} e^{-(x^2+y^2)/2}$ for the first excited state in both x- and y-directions ϕ_{11}. The problem is solved on $\Omega_{\mathbf{x}} = [-16,16]^2$ with mesh size $h = \frac{1}{16}$. For comparison of different methods and different time step size, the termination condition for steady state solution is uniformly chosen as $\max_{j,k} \frac{|\phi_{jk}^{n+1} - \phi_{jk}^n|}{\Delta t} < 10^{-6}$. Tables 5 and 6 show the computational time taken to get the ground state by using different methods and different time step sizes with $\kappa = 100$ for $\beta = 100$ and $\beta = 1000$, respectively. Furthermore, Fig. 2 visualizes the ground and first excited states for $\beta = 500$ and $\kappa = 50$ by using BESP with time step $\Delta t = 0.1$ and $\Delta t = 0.001$, respectively. We also compute their energy and chemical potential as $E_g = 32.2079$, $\mu_g = 41.7854$; $E_{10} := E(\phi_{10}) = E_{01} := E(\phi_{01}) = 34.6044$, $\mu_{10} := \mu(\phi_{10}) = \mu_{01} := \mu(\phi_{01}) = 43.8228$; and $E_{11} := E(\phi_{11}) = 37.0849$, $\mu_{11} := \mu(\phi_{11}) = 46.1402$.

From Tables 5, 6, Fig. 2 and additional experiments not shown here, the following observations are made:

(i) BESP and BEFD are implicit method, and energy diminishing is observed for both the linear and the nonlinear cases under any time step $\Delta t > 0$; where FESP is explicit and BFSP is implicit but can be solved explicitly, energy diminishing is observed only when the time step Δt satisfies a constraint.

(ii) For BESP, the computational time is almost constant in the example for different β and different time step $0.005 \leqslant \Delta t \leqslant 0.5$. Thus there is no need to bother on how to choose the time step. One can always choose $\Delta t = 0.5$ or $\Delta t = 0.1$ in practical computation. For FESP, only very small time step is allowed. When time step is decreased by half, the computational time is doubled. For BFSP, intermediate large time step is allowed. The introduction of the stabilization term allows larger time step to be chosen in practical computation. When the time step is chosen near the largest allowable time step, the computational time is much smaller than that in BESP. Furthermore, the growing rate of computational time with respect to time step size by using BFSP is faster than that of using BESP.

Table 5
Computational times for computing ground state in Example 2 by using different numerical schemes for $\beta = 100$

Numerical scheme	Δt	Computational time (s)	E_g	μ_g
BESP	0.5	597.6	26.92580539	33.292591
	0.25	622.6	26.92580539	33.292586
	0.1	637.3	26.92590539	33.292585
	0.05	661.8	26.92580539	33.292584
	0.01	805.9	26.92580539	33.292584
	0.0025	1290	26.92580539	33.292584
BFSP	0.1	52.1	26.9357459	33.410725
	0.05	56.4	26.9348784	33.405024
	0.025	63.7	26.9334524	33.395124
	0.01	84.9	26.9307326	33.373672
	0.005	117.2	26.9285960	33.352679
	0.001	372.3	26.9261198	33.312119
FESP	0.001	–	–	–
	0.0005	643.9	26.92580539	33.29258356
	0.00025	1304	26.92580539	33.29258357
	0.0001	3295	26.92580539	33.29258357

Table 6
Computational times for computing ground state in Example 2 by using different numerical schemes for $\beta = 1000$

Numerical scheme	Δt	Computational time (s)	E_g	μ_g
BESP	0.5	593.9	51.22028604	66.249024
	0.25	608.1	51.22028604	66.249017
	0.1	620.6	51.22028604	66.249013
	0.05	635.7	51.22028604	66.249011
	0.01	743.3	51.22028604	66.249010
	0.0025	1144	51.22028604	66.249010
BFSP	0.025	–	–	–
	0.01	79.9	51.2283083	66.376381
	0.005	106.1	51.2248581	66.344476
	0.0025	165.8	51.2223469	66.312619
	0.001	345.3	51.2208091	66.280800
	0.0005	648.6	51.2204428	66.266346
	0.00025	1251	51.2203292	66.258089
FESP	0.001	–	–	–
	0.0005	606.8	51.22028604	66.2490096
	0.00025	1306	51.22028604	66.2490096
	0.0001	3331	51.22028604	66.2490094

(iii) From the numerical values of energy and chemical potential calculated, BESP performs better than BFSP in terms of accuracy. In fact, for BESP, the energy and chemical potential are almost independent of the time step size, while for BFSP, better results are obtained when smaller time step is used.

(iv) Interior layers are observed in the first excited state when β is large (cf. Fig. 2). Multiscale structures are observed in both ground and first excited states. Furthermore, we also observed numerically

$$E(\phi_g) < E(\phi_{10}) = E(\phi_{01}) < E(\phi_{11}), \quad \mu(\phi_g) < \mu(\phi_{10}) = \mu(\phi_{01}) < \mu(\phi_{11}), \quad \beta \geqslant 0,$$
$$\lim_{\beta\to\infty} \frac{E(\phi_{10})}{E(\phi_g)} = \lim_{\beta\to\infty} \frac{E(\phi_{11})}{E(\phi_g)} = 1, \quad \lim_{\beta\to\infty} \frac{\mu(\phi_{10})}{\mu(\phi_g)} = \lim_{\beta\to\infty} \frac{\mu(\phi_{11})}{\mu(\phi_g)} = 1.$$

The relations $\phi_{10}(x,y) = \phi_{01}(y,x)$, $E(\phi_{10}) = E(\phi_{01})$ and $\mu(\phi_{10}) = \mu(\phi_{01})$ are due to $V(x,y) = V(y,x)$.

4.3. Results in 3D

Example 3. Ground and first excited states in 3D under a combined harmonic and optical lattice potential, i.e., we take $d = 3$ and $V(x,y,z) = \frac{1}{2}(x^2+y^2+z^2) + 50\left[\sin^2(\frac{\pi x}{4}) + \sin^2(\frac{\pi y}{4}) + \sin^2(\frac{\pi z}{4})\right]$ in (1.3). The choice of the optical lattice depth and nonlinearity is motivated from the physics literatures [21,23]. The initial data (3.4) is chosen as (2.8) for computing ground state ϕ_g, and as $\phi_0(x,y,z) = \frac{\sqrt{2}x}{\pi^{3/4}} e^{-(x^2+y^2+z^2)/2}$ for the first excited state in x-direction ϕ_{100}, and as $\phi_0(x,y,z) = \frac{2xy}{\pi^{3/4}} e^{-(x^2+y^2+z^2)/2}$ for the first excited state in x- and y-directions ϕ_{110}, and as $\phi_0(x,y,z) = \frac{2^{3/2}xyz}{\pi^{3/4}} e^{-(x^2+y^2+z^2)/2}$ for the first excited state in x-, y- and z-directions ϕ_{111}. The problem is solved on $\Omega_{\mathbf{x}} = [-8,8]^3$ by using BESP with mesh size $h = \frac{1}{8}$. The time step is chosen as $\Delta t = 0.1$ for computing ground state and $\Delta t = 0.001$ for computing the first excited states. Fig. 3 plots the isosurfaces of the ground state for $\beta = 100$, 800 and 6400. Fig. 4 shows the isosurfaces of the first excited states for $\beta = 100$. Table 7 lists the energy and chemical potential for ground state and first excited states for different β. In fact, BFSP gives similar results when $\Delta t = 0.01$ for computing the ground state and $\Delta t = 0.001$ for computing the first excited states.

From Table 7, Figs. 3, 4 and additional experiments not shown here, the following observations are made:

(i) The BESP and BFSP are capable for computing ground and first excited states in BEC in 3D when the solutions have multiscale structures.

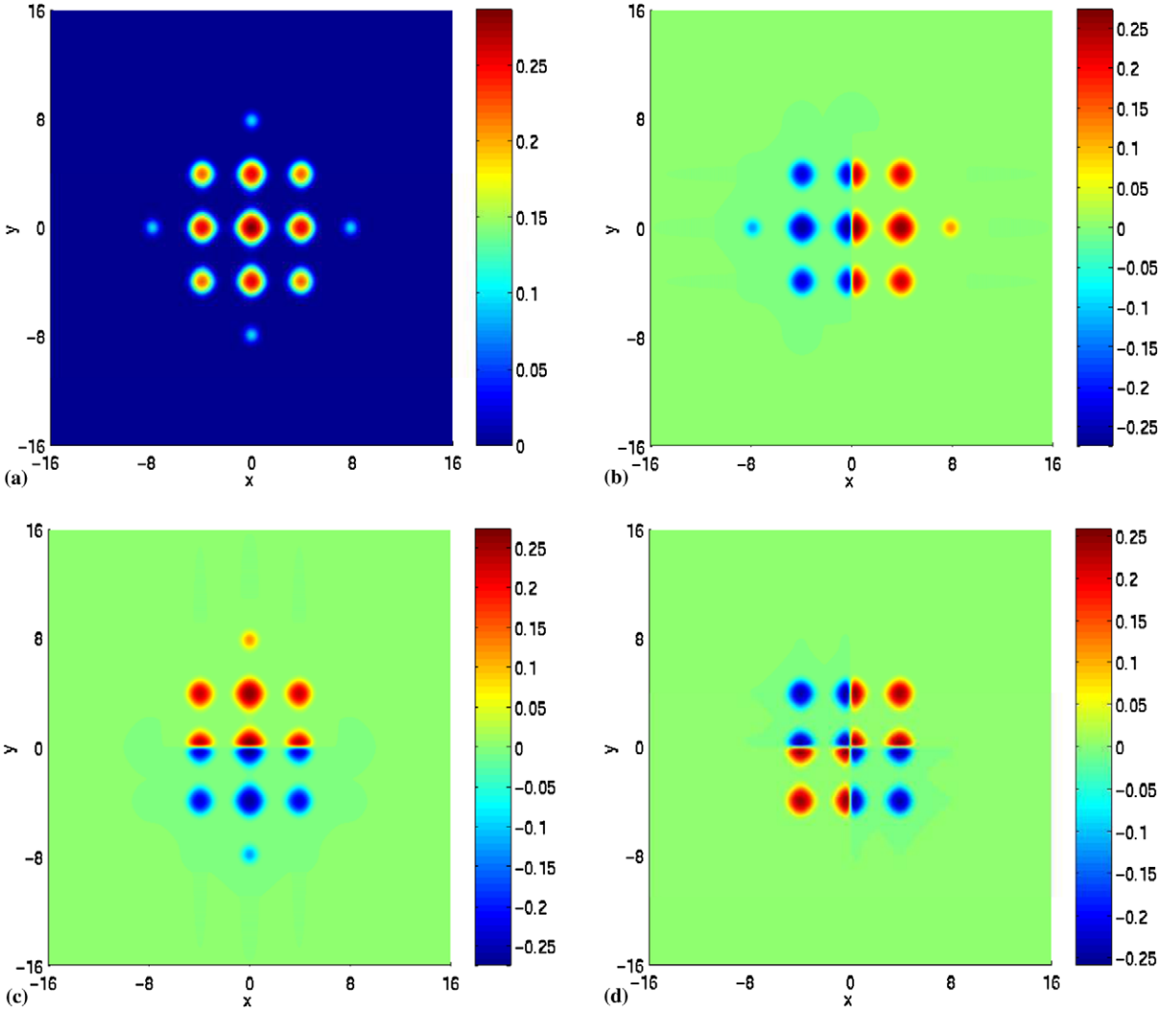

Fig. 2. Top views of numerical results in Example 2 for $\beta = 500$: (a) ground state ϕ_g; (b) first excited state in x-direction ϕ_{10}; (c) first excited state in y-direction ϕ_{01}; (d) first excited state in both x- and y-directions ϕ_{11}.

(ii) Interior layers are observed in the first excited state when β is large (cf. Fig. 4). Multiscale structures are observed in both ground and first excited states under an optical lattice potential. Furthermore, we also observed numerically:

$$E(\phi_g) < E(\phi_{100}) = E(\phi_{010}) = E(\phi_{001}) < E(\phi_{110}) = E(\phi_{101}) = E(\phi_{011}) < E(\phi_{111}),$$

$$\mu(\phi_g) < \mu(\phi_{100}) = \mu(\phi_{010}) = \mu(\phi_{001}) < \mu(\phi_{110}) = \mu(\phi_{101}) = \mu(\phi_{011}) < \mu(\phi_{11}), \quad \beta \geqslant 0,$$

$$\lim_{\beta\to\infty} \frac{E(\phi_{100})}{E(\phi_g)} = \lim_{\beta\to\infty} \frac{E(\phi_{110})}{E(\phi_g)} = \lim_{\beta\to\infty} \frac{E(\phi_{111})}{E(\phi_g)} = 1,$$

$$\lim_{\beta\to\infty} \frac{\mu(\phi_{100})}{\mu(\phi_g)} = \lim_{\beta\to\infty} \frac{\mu(\phi_{110})}{\mu(\phi_g)} = \lim_{\beta\to\infty} \frac{\mu(\phi_{111})}{\mu(\phi_g)} = 1.$$

The relations $E(\phi_{100}) = E(\phi_{010})$ and $\mu(\phi_{100}) = \mu(\phi_{010})$ are due to $V(x, y, z) = V(y, x, z)$.

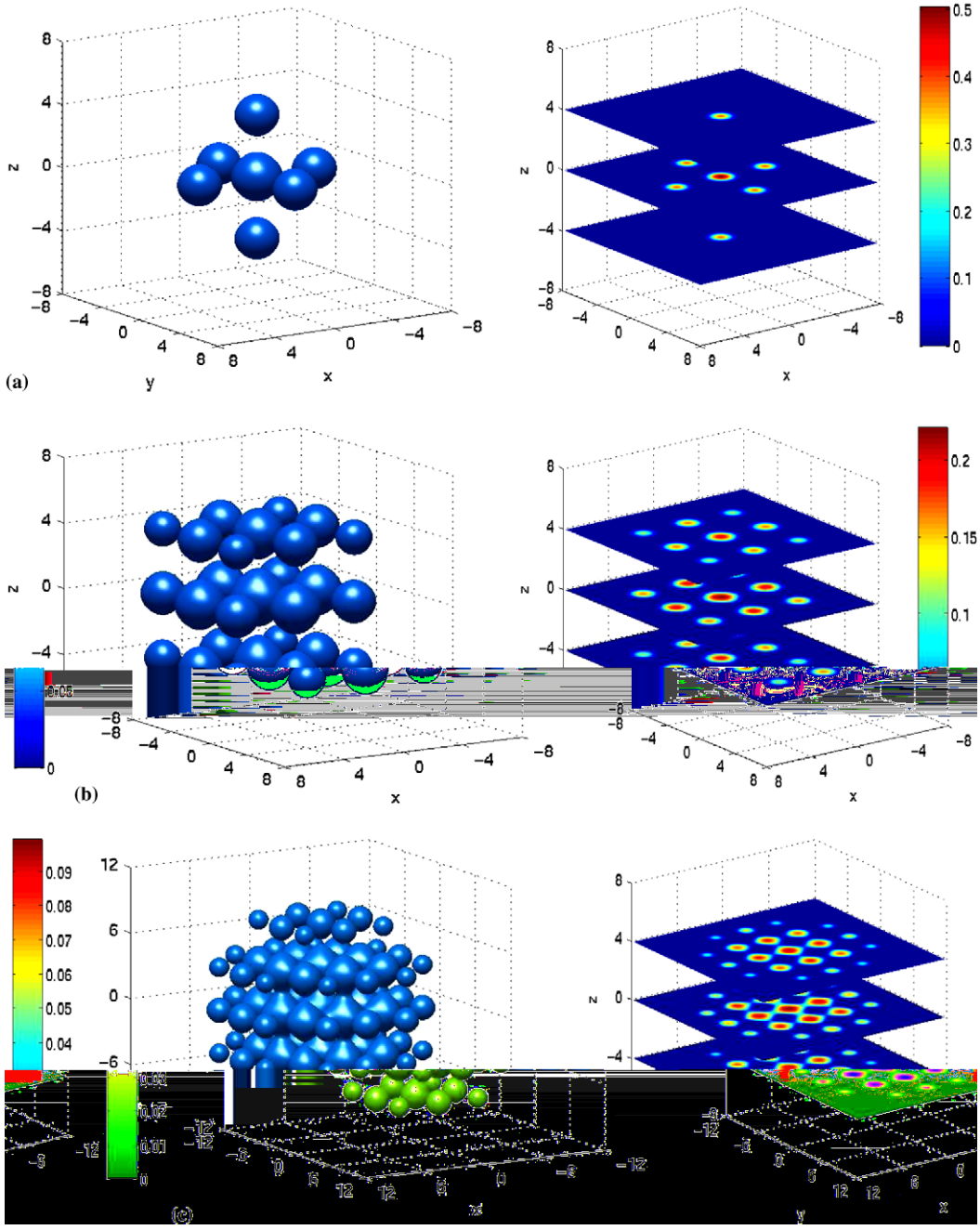

Fig. 3. Isosurfaces (left column) and their corresponding slice views (right column) for ground states in Example 3 for different β: (a) $\beta = 100$; (b) $\beta = 800$; (c) $\beta = 6400$.

5. Conclusion

We have presented two efficient and spectrally accurate numerical methods for computing the ground and first excited states in BEC. The methods are based on applying sine-pseudospectral discretization for spatial derivatives and backward Euler (BESP) for backward/forward Euler for linear/nonlinear terms for time deriv-

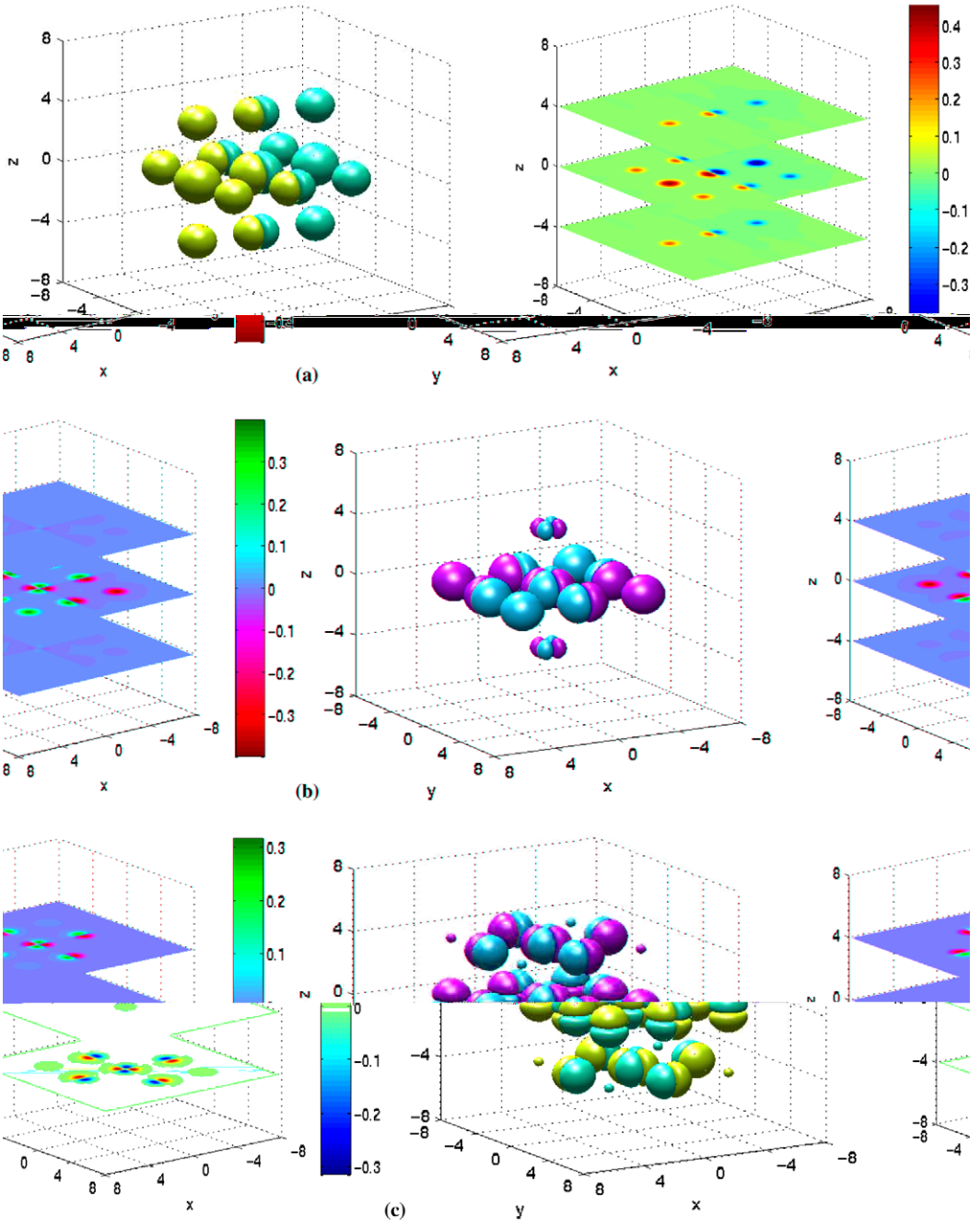

Fig. 4. Isosurfaces (left column) and their corresponding slice views (right column) for the first excited states in Example 3 for $\beta = 100$: (a) first excited state in x-direction ϕ_{100}; (b) first excited state in x- and y-directions ϕ_{110}; (c) first excited state in x-, y- and z-directions ϕ_{111}.

atives in a normalized gradient flow. Both BESP and BFSP are demonstrated to be spectrally accurate for computing the ground and first excited states in BEC. Furthermore, BESP is energy diminishing for any time step $\Delta t > 0$, where BFSP is under a constraint on the time step Δt. Thus larger mesh size and time step can be chosen in practical computation when high accuracy is required. Therefore, the computational memory and computational time can be saved significantly, especially in 2D and 3D.

Table 7
Energy and chemical potential of ground and first excited states in Example 3 for different β

β	E_g, μ_g	$E(\phi_{100})$, $\mu(\phi_{100})$	$E(\phi_{110})$, $\mu(\phi_{110})$	$E(\phi_{111})$, $\mu(\phi_{111})$
0	11.6439, 11.6439	19.2450, 19.2450	26.8462, 26.8462	34.4473, 34.4473
10	15.9852, 19.1506	21.0720, 22.5140	27.8833, 28.6755	35.1742, 35.7086
25	18.6574, 21.3997	22.9316, 25.6428	28.9665, 30.6305	35.7780, 36.8161
100	23.2356, 27.4757	27.1939, 30.4217	31.2498, 34.3400	36.7368, 38.4113
200	26.1956, 30.6831	29.7009, 33.8039	33.7883, 38.0816	38.2237, 40.9526
800	33.8023, 40.4476	36.7106, 42.9200	39.6478, 45.3623	42.6474, 47.8224
3200	45.2035, 54.9862	47.4672, 56.8902	50.3045, 60.2456	52.7426, 62.3855
6400	52.4955, 63.7149	54.8717, 66.3303	58.0720, 70.5760	60.3200, 72.5372

Based on our extensive comparisons in terms of accuracy and computational time, we make the following suggestions on how to choose numerical methods:

(i) If high accuracy is crucial in computing ground states in BEC, e.g. under an optical lattice potential or in a rotational frame, we always recommend to use BESP or BFSP. If one does not want to be bothered on how to choose the time step, BESP with time step $\Delta t = 0.5$ or $\Delta t = 0.1$ is a very good choice. Of course, if one can find the largest allowable time step for BFSP, then BFSP is a much better choice since it needs much less computational time.
(ii) For computing first excited states in BEC, in order to suppress the round-off error in FST and IFST such that the numerical solution is an odd function, small time step is required. Thus we recommend BFSP for computation.
(iii) Here we also suggest a combined method of BESP and BFSP which enjoys high efficiency of BFSP and better resolution of BESP: First apply BFSP for the gradient flow evolution to reach a steady state solution, followed by applying BESP at a later stage to refine the solution. This scheme gives a highly accurate solution as BESP does, with much less computational time taken as compared with applying BESP for the whole procedure.

Acknowledgments

W.B. acknowledges support by the National University of Singapore Grant No. R-146-000-081-112 and helpful discussion with Professor Jie Shen. I.C. acknowledges support by the National Science Council of the Republic of China, Grant No. NSC94-2115-M-002-017. This work was partially done when the first author was visiting the Institute for Mathematical Sciences, National University of Singapore and Department of Mathematics, Capital Normal University in 2005, and when the second author was visiting the Department of Computational Science, National University of Singapore.

Appendix A. An algorithm for implementing BESP

(i) Compute $\phi_j^0 = \phi_0(x_j)$ $(j = 0,1,\ldots,M)$. Let $n = 0$.
(ii) Repeat n: until convergence.
(iii) Compute $b_{\max}$ and $b_{\min}$ via (3.18) and $\alpha = \alpha_{\text{opt}}$ via (3.19). Take discrete sine transform (DST) for $\{\phi_j^n\}_{j=1}^{M-1}$ and obtain $\{(\widehat{\phi^n})_l\}_{l=1}^{M-1}$. Let $m = 0$ and set $\phi_j^{*,m} = \phi_j^n$ $(j = 0,1,\ldots,M)$.
(iv) Repeat m: until convergence.
(v) Compute G_j^m via (3.11) and take DST for $\{G_j^m\}_{j=1}^{M-1}$ and obtain $\{(\widehat{G^m})_l\}_{l=1}^{M-1}$.
(vi) Compute $(\widehat{\phi^{*,m+1}})_l$ via (3.12).
(vii) Take inverse discrete sine transform (IDST) for $\{(\widehat{\phi^{*,m+1}})_l\}_{l=1}^{M-1}$ and obtain $\{\phi_j^{*,m+1}\}_{j=1}^{M-1}$.
(viii) If $\max_{1\leqslant j\leqslant M-1}|\phi_j^{*,m+1} - \phi_j^{*,m}| > \epsilon_0$ (e.g. 10^{-8}), set $m := m + 1$, go to step (v); otherwise go to next step.
(ix) Compute ϕ_j^{n+1} via (3.7) with $\phi_j^* = \phi_j^{*,m+1}$.
(x) If $\max_{1\leqslant j\leqslant M-1}|\phi_j^{n+1} - \phi_j^n| > \epsilon_1$ (e.g. 10^{-6}), set $n := n + 1$, go to step (iii); otherwise stop and $\{\phi_j^{n+1}\}_{j=1}^{M-1}$ is the result.

Appendix B. An algorithm for implementing BFSP

(i) Compute $\phi_j^0 = \phi_0(x_j)$ $(j = 0,1,\ldots,M)$. Let $n = 0$.
(ii) Repeat n: until convergence.
(iii) Compute $b_{\max}$ and $b_{\min}$ via (3.18) and $\alpha = \alpha_{\text{opt}}$ via (3.19). Take DST for $\{\phi_j^n\}_{j=1}^{M-1}$ and obtain $\{(\widehat{\phi^n})_l\}_{l=1}^{M-1}$.
(iv) Compute G_j^n via (3.11) with $m = n$ and take DST for $\{G_j^n\}_{j=1}^{M-1}$ and obtain $\{(\widehat{G^n})_l\}_{l=1}^{M-1}$.
(v) Compute $(\widehat{\phi^{*,n+1}})_l$ via (3.12) with $m = n$.
(vi) Take IDST for $\{(\widehat{\phi^{*,n+1}})_l\}_{l=1}^{M-1}$ and obtain $\{\phi_j^{*,n+1}\}_{j=1}^{M-1}$.
(vii) Compute ϕ_j^{n+1} via (3.7) with $\phi_j^* = \phi_j^{*,n+1}$.
(viii) If $\max_{1\leqslant j\leqslant M-1}|\phi_j^{n+1} - \phi_j^n| > \epsilon_1$ (e.g. 10^{-6}), set $n := n + 1$, go to step (iii); otherwise stop and $\{\phi_j^{n+1}\}_{j=1}^{M-1}$ is the result.

References

[1] S.K. Adhikari, Numerical solution of the two-dimensional Gross–Pitaevskii equation for trapped interacting atoms, Phys. Lett. A 265 (2000) 91–96.
[2] A. Aftalion, Q. Du, Vortices in a rotating Bose–Einstein condensate: critical angular velocities and energy diagrams in the Thomas–Fermi regime, Phys. Rev. A 64 (2001) (article 063603).
[3] M.H. Anderson, J.R. Ensher, M.R. Matthewa, C.E. Wieman, E.A. Cornell, Observation of Bose–Einstein condensation in a dilute atomic vapor, Science 269 (1995) 198–201.
[4] W. Bao, Ground states and dynamics of multi-component Bose–Einstein condensates, Multiscale Model. Simul. 2 (2004) 210–236.
[5] W. Bao, Q. Du, Computing the ground state solution of Bose–Einstein condensates by a normalized gradient flow, SIAM J. Sci. Comput. 25 (2004) 1674–1697.
[6] W. Bao, D. Jaksch, P.A. Markowich, Numerical solution of the Gross–Pitaevskii equation for Bose–Einstein condensation, J. Comput. Phys. 187 (2003) 318–342.
[7] W. Bao, F.Y. Lim, Y. Zhang, Energy and chemical potential asymptotics for the ground state of Bose–Einstein condensates in the semiclassical regime, Trans. Theory Stat. Phys. (in press).
[8] W. Bao, W. Tang, Ground state solution of trapped interacting Bose–Einstein condensate by directly minimizing the energy functional, J. Comput. Phys. 187 (2003) 318–342.
[9] W. Bao, H. Wang, P.A. Markowich, Ground, symmetric and central vortex states in rotating Bose–Einstein condensates, Commun. Math. Sci. 3 (2005) 57–88.
[10] G. Baym, C.J. Pethick, Ground-state properties of magnetically trapped Bose-condensed rubidium gas, Phys. Rev. Lett. 76 (1996) 6–9.
[11] S.-M. Chang, W.-W. Lin, S.-F. Shieh, Gauss–Seidel-type methods for energy states of a multi-component Bose–Einstein condensate, J. Comput. Phys. 202 (2005) 367–390.
[12] S.M. Chang, C.S. Lin, T.C. Lin, W.W. Lin, Segregated nodal domains of two-dimensional multispecies Bose–Einstein condensates, Physica D 196 (2004) 341–361.
[13] M.M. Cerimele, M.L. Chiofalo, F. Pistella, S. Succi, M.P. Tosi, Numerical solution of the Gross–Pitaevskii equation using an explicit finite-difference scheme: an application to trapped Bose–Einstein condensates, Phys. Rev. E 62 (2000) 1382–1389.
[14] M.L. Chiofalo, S. Succi, M.P. Tosi, Ground state of trapped interacting Bose–Einstein condensates by an explicit imaginary-time algorithm, Phys. Rev. E 62 (2000) 7438–7444.
[15] K.B. Davis, M.O. Mewes, M.R. Andrews, N.J. van Druten, D.S. Durfee, D.M. Kurn, W. Ketterle, Bose–Einstein condensation in a gas of sodium atoms, Phys. Rev. Lett. 75 (1995) 3969–3973.
[16] R.J. Dodd, Approximate solutions of the nonlinear Schrödinger equation for ground and excited states of Bose–Einstein condensates, J. Res. Natl. Inst. Stan. 101 (1996) 545–552.
[17] M. Edwards, K. Burnett, Numerical solution of the nonlinear Schrodinger equation for small samples of trapped neutral atoms, Phys. Rev. A 51 (1995) 1382–1386.
[18] M. Edwards, P.A. Ruprecht, K. Burnett, R.J. Dodd, C.W. Clark, Collective excitations of atomic Bose–Einstein condensates, Phys. Rev. Lett. 77 (1996) 1671–1674.
[19] A. Gammal, T. Frederico, L. Tomio, Improved numerical approach for the time-independent Gross–Pitaevskii nonlinear Schrödinger equation, Phys. Rev. E 60 (1999) 2421–2424.
[20] G.H. Golub, C.F. Van Loan, Matrix Computations, Johns Hopkins University Press, Baltimore, MD, 1989.
[21] M. Greiner, O. Mandel, T. Esslinger, T.W. Hänsch, I. Bloch, Quantum phase transition from a superfluid to a Mott insulator in a gas of ultracold atoms, Nature 415 (2002) 39–44.
[22] E.P. Gross, Structure of a quantized vortex in boson systems, Nuovo. Cimento. 20 (1961) 454–477.
[23] T.L. Ho, Spinor Bose condensates in optical traps, Phys. Rev. Lett. 81 (1998) 742–745.
[24] D. Jaksch, C. Bruder, J.I. Cirac, C.W. Gardiner, P. Zoller, Cold bosonic atoms in optical lattices, Phys. Rev. Lett. 81 (1998) 3108–3111.

[25] C. Kollath, U. Schollwock, J. von Delft, W. Zwerger, One-dimensional density waves of ultracold bosons in an optical lattice, Phys. Rev. A 71 (2005) (article 053606).
[26] E.H. Lieb, R. Seiringer, J. Yugvason, Bosons in a trap: a rigorous derivation of the Gross–Pitaevskii energy functional, Phys. Rev. A 61 (2000) 3602.
[27] L.P. Pitaevskii, Vortex lines in an imperfect Bose gas, Soviet Phys. JETP 13 (1961) 451–454.
[28] L.P. Pitaevskii, S. Stringari, Bose–Einstein Condensation, Clarendon Press, Oxford, 2003.
[29] D.S. Rokhsar, Vortex stability and persistent currents in trapped Bose-gas, Phys. Rev. Lett. 79 (1997) 2164–2167.
[30] P.A. Ruprecht, M.J. Holland, K. Burrett, M. Edwards, Time-dependent solution of the nonlinear Schrodinger equation for Bose-condensed trapped neutral atoms, Phys. Rev. A 51 (1995) 4704–4711.
[31] B.I. Schneider, D.L. Feder, Numerical approach to the ground and excited states of a Bose–Einstein condensated gas confined in a completely anisotropic trap, Phys. Rev. A 59 (1999) 2232.
[32] C. Tozzo, M. Kramer, F. Dalfovo, Stability diagram and growth rate of parametric resonances in Bose–Einstein condensates in one-dimensional optical lattices, Phys. Rev. A 72 (2005) (article 023613).
[33] A.H. Zhou, An analysis of finite-dimensional approximations for the ground state solution of Bose–Einstein condensates, Nonlinearity 17 (2004) 541–550.